Channel Rich RuCu Nanosheets for pH-Universal Overall Water Splitting Electrocatalysis

Qing Yao, Nan Zhang, Jian Yang, Mingzi Sun, Qi Shao, Bolong Huang* and Xiaoqing Huang*

Abstract: Developing efficient overall water splitting electrocatalysts applicable in pH-universal electrolytes is extremely critical for the practical applications. Herein, we demonstrated that the channel rich RuCu snowflake-like nanosheets (NSs) composed of crystallized Ru and amorphous Cu can be adopted as efficient electrocatalysts for oxygen evolution reaction, hydrogen evolution reaction as well as overall water splitting in pH-universal electrolytes. The optimized RuCu NSs/C-350 °C and RuCu NSs/C-250 °C show attractive activities of oxygen evolution reaction (OER) and hydrogen evolution reaction (HER) with low overpotentials and small Tafel slopes, respectively. When applied to overall water splitting, the optimized RuCu NSs/C can reach 10 mA cm^{-2} at cell voltages of only 1.49, 1.55, 1.49 and 1.50 V in 1 M KOH, 0.1 M KOH, 0.5 M H_2SO_4 and 0.05 M H_2SO_4, respectively, much lower than those of commercial Ir/C||Pt/C. DFT calculations reveal that the channel-rich structure will substantially alleviate the t_{2g}-e_g splitting, which minimized the surface Coulomb repulsion to achieve fast electron-transfer for a barrier-free process. The balanced electronic structure between Ru and Cu will deliver the universal electroactivity for water-splitting. The optimized electrolyzer also exhibits superior durability with small potential change after up to 45 h in 1 M KOH, showing a class of efficient bifunctional electrocatalysts for overall water splitting.

Water electrolysis is considered as one of the most promising approaches to produce zero-carbon hydrogen (H_2) with high purity from water.[1-4] Despite tremendous efforts have been devoted, there are still critical bottlenecks that limit practical applications of water electrolysis. For instance, the half reaction of water electrolysis—oxygen evolution reaction (OER) is troubled by sluggish kinetics, resulting in high overpotential.[5, 6] In recent years, earth-abundant transition metals have attracted extensive research attention, but they are still seriously hampered due to their poor activity and durability.[7-10] Iridium (Ir) based and platinum (Pt) based electrocatalysts exhibit good performance in OER and hydrogen evolution reaction (HER), respectively, while the demerits including scarcity and high cost still limit their large-scale practical applications.[11-14]

Ruthenium (Ru), due to the advantages of the cheapest among platinum group metal and excellent performance in many applications such as N_2 electrochemical reduction and selective hydrogenation, has attracted intensive attention.[15, 16] Significantly, it has also been proved that Ru-based electrocatalysts are active in both HER and OER. [17-20] For instance, Su and coworkers have obtained Cu-doped RuO_2 hollow porous polyhedra through one-step annealing of Ru-exchanged Cu-BTC derivatives, which showed remarkable OER performance in 0.5 M H_2SO_4.[21] Liu and colleagues have synthesized multi-heterogeneous Ni@Ni_2P-Ru nanorods showing excellent electrocatalytic HER performance.[17] Despite those progress, the design of efficient Ru-based applicable electrocatalysts for OER, HER as well as overall water splitting in pH-universal conditions has been still largely unexplored.

From the viewpoint of structure, two-dimensional (2D) structure can provide more opportunities for enhancing the electrochemical performance by offering larger surface and exposing more atoms serving as active sites.[22-25] Herein, we report a facile wet chemical method to synthesize channel rich RuCu nanosheets composed of crystallized Ru and amorphous Cu with many accessible channels (denoted as RuCu NSs). The optimized RuCu NSs exhibit enhanced electrochemical performance towards OER and HER. In details, the optimized RuCu NSs/C-350 °C show the attractive activity of OER, while the RuCu NSs/C-250 °C show the attractive activity of HER. Importantly, when applied to overall water splitting, the optimized RuCu NSs/C deliver small onset potential and achieve 10 mA cm^{-2} at 1.48, 1.55 V, 1.49 V and 1.50 V in 1 M, 0.1 M KOH, 0.5 M and 0.05 M H_2SO_4, respectively, much lower than those of RuCu NPs/C and commercial Ir/C||Pt/C. The optimized electrolyzer also displays superior stability with limited overpotential change after long-term durability test.

The preparation of RuCu NSs was realized by the one-pot method by using ruthenium(III) chloride hydrate ($RuCl_3 \cdot xH_2O$) and copper(II) chloride dihydrate ($CuCl_2 \cdot 2H_2O$) as metal precursors, phloroglucinol as reducing agent and oleylamine along with octadecene as mixed solvent (see Supporting Information for details). Detailed characterizations of the RuCu NSs are shown in **Figure 1** and **Figures S1-S3**. Typical transmission electron microscopy (TEM) (**Figure 1a**) and high-angle annular dark-field scanning TEM (HAADF-STEM) images show that the obtained products with snowflake-like shape are uniform with the average size of 48.7 nm

[a] Q. Yao, N. Zhang, J. Yang, Q. Shao and Prof. X. Huang,
College of Chemistry, Chemical Engineering and Materials Science Soochow University
No.199, Ren'ai Road, Suzhou 215123, Jiangsu, China
E-mail: hxq006@suda.edu.cn
[b] M. Sun and Prof. B. Huang
Department of Applied Biology and Chemical Technology, The Hong Kong Polytechnic University, Hung Hom, Kowloon, Hong Kong SAR, China
E-mail: bhuang@polyu.edu.hk

Supporting information for this article is given via a link at the end of the document.

(**Figure 1b, Figure S1**). The thickness is ~ 6 nm, as determined by atomic force microscopy (AFM) (**Figure 1c, Figure S2**). Interestingly, abundant accessible channels can be observed in those RuCu NSs (**Figure 1d**), which is beneficial for enhancing the electrochemical performance by increasing surface area and boosting mass transfer.[19] The atomic ratio of Ru/Cu is determined to be 5.5/1 by energy dispersive X-ray (EDX) spectroscopy (**Figure S3a**). As manifested by the elemental mappings (**Figure 1e**) and line-scanning profiles (**Figure S3b**), the Ru and Cu are uniformly distributed in the NSs, further confirming the successful synthesis of bimetallic RuCu NSs. The X-ray diffraction (XRD) pattern shows that all of the diffraction peaks can be indexed to the pattern of hexagonal-close-packed (*hcp*) Ru (JCPDS Card.06-0663) and no obvious peak shift is observed on RuCu NSs relative to metallic Ru (**Figure 1f**). Lattice spacing is measured to be 0.23 nm, corresponding to the (100) facet of Ru and no lattice fringe of Cu is observed (**Figure 1g**). The associated fast Fourier transform (FFT) (inset of **Figure 1g**) also clearly showed bright spots that represent the crystallized Ru. All the results indicate that RuCu NSs are composed of crystallized Ru and amorphous Cu.[26, 27]

To optimize the catalytic performance, the channel rich RuCu NSs were loaded on carbon black (**Figure S4**) and annealed in air for 1 h at different temperatures (i. e., 250 °C, 300 °C and 350 °C, denoted as RuCu NSs/C-T, T = 250 °C, 300 °C, 350 °C, respectively) (**Figure S5a,b**). Combined with XRD patterns of different RuCu NSs/C-T (**Figure S6**), 250 °C is a proper temperature to remove oleylamine residues on the surface with largely maintaining Ru in the metallic state and 350 °C is proper to convert most of Ru to Ru^{4+}. We used three-electrode system to test OER and HER performance in 1 M KOH with carbon rod as the counter electrode, saturated calomel electrode as the reference electrode and glassy carbon electrode as the working electrode. All potentials were calibrated to the reversible hydrogen electrode (RHE). It was found that RuCu NSs/C-350 °C show the best OER activity, while RuCu NSs/C-250 °C show the best HER activity (**Figure S7a,b**).

We then evaluated the OER performances of RuCu NSs/C-350 °C in both alkaline and acidic conditions. As-prepared RuCu NPs/C annealed in air for 1h at 350 °C (denoted as RuCu NPs/C-350 °C) (**Figure S8**), commercial Pt/C and Ir/C were selected as references for comparison. We summarized OER polarization curves in different electrolytes in **Figure 2a-2d.** Compared with RuCu NPs/C-350 °C and commercial catalysts, RuCu NSs/C-350 °C exhibit much enhanced OER activity. In details, the overpotentials of RuCu NSs/C-350 °C at 10 mA cm^{-2} were relatively small with only 234, 276, 236, 240 mV at 1 M, 0.1 M KOH, 0.5 M and 0.05 M H_2SO_4, respectively (**Figure 2e**). Moreover, the Tafel plots in above four electrolytes showed that the slopes of RuCu NSs/C-350 °C were even smaller than those of RuCu NPs/C-350 °C, Ir/C and

Pt/C, indicating the favorable reaction kinetics in both alkaline and acidic condition (**Figure S9**). The electrochemical surface area (ECSA) of RuCu NSs/C-350 °C is almost the same to that of RuCu NPs/C-350 °C, while the electrochemical impedance spectroscopy (EIS) showed that RuCu NSs/C-350 °C has the fastest electron transfer (**Figure S10**).[28] Significantly, the high OER stability of RuCu NSs/C-350 °C in 1 M KOH and 0.5 M H_2SO_4 were also confirmed by chronoamperometry measurement. In 1 M KOH there was a very small increase during 21.5 h test and limited increase during 13.5 h test in 0.5 M H_2SO_4 at 5 mA cm^{-2}, **(Figure S11, 12)**. Excitingly, the performance of RuCu NSs/C-350 °C can be maintained in both 1 M KOH and 0.5 M H_2SO_4 at 10 mA cm^{-2} for 12 h (**Figure 2f, Figure S13**). As shown in **Figures S14,** the morphology of RuCu NSs/C-350 °C after long time chronopotentiometry test in 1 M KOH was largely maintained with no obvious phase change. The atomic ratio of Ru/Cu increased from 5.5:1 to 9.8:1, indicating partial Cu dissolution during the OER process. Both HRTEM and X-ray photoelectron spectrum (XPS) analyses showed that the surface structure was hardly changed after OER stability tests, confirming the high stability of RuCu NSs-350 °C towards OER.

We also explored the HER performance of RuCu NSs/C-250 °C in different electrolytes (**Figure 3**). As shown in **Figure 3a-3d,** RuCu NSs/C-250 °C exhibited the best HER activity in both acidic and alkaline conditions. In details, the overpotentials at 10 mA cm^{-2} in 1 M KOH, 0.1 M KOH, 0.5 M H_2SO_4 and 0.05 M H_2SO_4 are only 20, 40, 19 and 27 mV, respectively, outperforming those of RuCu NPs/C-250 °C (111, 139, 102 and 106 mV), Pt/C (60, 67, 24 and 30 mV) and Ir/C (70, 72, 37 and 38 mV) (**Figure 3e**). In particular, the Tafel slopes of RuCu NSs/C-250 °C in alkaline conditions (15.3 and 22.3 mV dec^{-1}) were obviously lower than those of RuCu NPs/C-250 °C (73.1 and 82.8 mV dec^{-1}), Pt/C (39.8 and 42.0 mV dec^{-1}) and Ir/C (42.4 and 48.1 mV dec^{-1}), suggesting that the kinetics of RuCu NSs/C-250 °C becomes dominant during HER process in alkaline conditions (**Figure S15**). The Tafel slopes in acidic condition turn out that the HER process follows Volmer-Tafel pathway on RuCu NSs/C-250 °C and recombination of chemisorbed hydrogen atoms is the rate-determining step.[29] RuCu NSs/C-250 °C also has the lowest electric resistance than other catalysts (**Figure S16**).

Based on the high activity in both OER and HER, we further tested the overall water splitting by choosing RuCu NSs/C-350 °C as anode and RuCu NSs/C-250 °C as the cathode in two-electrode system. RuCu NPs/C and Ir/C||Pt/C were chosen as reference. The corresponding polarization curves were presented in **Figure 4** We can see that RuCu NSs/C exhibits much-enhanced performance, where only 1.49 V, 1.55 V, 1.49 V, 1.50 V are needed at 10 mA cm^{-2} in 1 M KOH, 0.1 M KOH, 0.5 M H_2SO_4 and 0.05 M H_2SO_4, respectively. The cell voltages of the

RuCu NSs/C are much smaller than those of RuCu NPs/C (1.605, 1.689, 1.615 and 1.630 V) and Ir/C||Pt/C (1.56 V, 1.66 V, 1.56 V and 1.57 V) in the same conditions, even smaller than the most state-of-the-art bifunctional electrocatalysts (**Figure 4b, Table S1**) Except for the reduced potentials, RuCu NSs/C also delivered sharply lower Tafel slopes (**Figure 4c, Figure S17**) and higher durability, which can maintain nearly 45 h chronopotentiometry test in 1 M KOH and nearly 20.5 h in 0.5 M H_2SO_4 at 5 mA cm^{-2} (**Figure S18, 19**). Even at 10 mA cm^{-2}, the performances of RuCu NSs/C can be maintained in both 1 M KOH and 0.5 M H_2SO_4 (**Figure 4d, Figure S20**). In addition, the voltage differences (ΔV) between HER and OER in different electrolytes (**Figure S21**) are almost equal to the cell voltages of RuCu NSs/C for overall water splitting, showing a steady process for water splitting.[30]

To further figure out the origin of the enhanced performance, we carried XPS to explore the surface properties of untreated RuCu NSs/C, RuCu NSs/C-250 °C and RuCu NSs/C-350 °C. In Ru $3p_{3/2}$ spectrum, peaks centered at 461.8 eV, 463.7 eV and 465.5 eV can be assigned to Ru^0, Ru^{4+} and Ru^{n+} (n>4), respectively (**Figure 5a**). Compared with untreated RuCu NSs/C, Ru 3p spectra of RuCu NSs/C-250 °C and RuCu NSs/C-350 °C showed an apparent shift to the higher binding energy, indicating the oxidation of Ru on the surface.[31] Notably, the ratio of Ru^{4+}/Ru^0 for untreated RuCu NSs is limited. When increasing the annealing temperature from 250 °C to 350 °C, Ru^{4+}/Ru^{0+} grown progressively, especially for RuCu NSs/C-350 °C with the ratio reaching 0.76 (**Figure 5b, Table S2**). This trend of Ru^{4+}/Ru^{0+} is in line with the OER performance and is consistent with the study that Ru^{4+} is the active site for promoting OER.[32-34] In addition to Ru 3p spectrum, Cu 2p spectrum reveals the coexistence of $Cu^{0/1+}$ and Cu^{2+}. In details, the binding energy at 932.8 eV is assigned to $Cu^{0/1+}$ and that at 934.7 eV is assigned to Cu^{2+} (**Figure 5c**). Similarly, the ratio of $Cu^{2+}/Cu^{0/1+}$ increased with increasing the annealing temperature (**Figure 5d, Table S2**). However, Cu 2p spectra of RuCu NSs-250 °C and RuCu NSs-350 °C shifted to lower binding energy, which can be attributed to the electron transfer from Ru to Cu and is also consistent with the result of Cu LMM Auger spectrum (**Figure S24**). To explore the synergistic effect between crystallized Ru and amorphous Cu, we etched the Cu of RuCu NSs/C (denoted as RuCu NSs/C-etch), where the RuCu NSs/C-etch-350 °C shows reduced OER activities (**Figure S22-S23**). We deduce that the amorphous Cu might optimize the adsorption energy of intermediates for enhanced OER catalysis. To better exhibit HER performance, we annealed pristine RuCu NSs/C in air at 250 °C to obtain clean surface and keep Ru element of RuCu NSs/C in Ru^0 at a large scale simultaneously, since the Ru^0 is good at water dissociation and the binding energy of Ru-H is moderate.[35] Therefore, in our work, we can conclude that

both the higher ratio of Ru^{4+}/Ru^{0} and $Cu^{2+}/Cu^{0/1+}$, together with the synergistic effect between Ru and Cu are key factors to enhance the OER activity. The abundant Ru^{0} in channel rich 2D RuCu NSs is the main factor that enhances HER activity.

In summary, we have successfully prepared the channel rich RuCu snowflake-like NSs composed of crystallized Ru and amorphous Cu. Due to the structural merits, the RuCu NSs exhibit superior HER and OER performances in both acidic and alkaline conditions. Significantly, the optimized RuCu NSs/C shows excellent performance in overall water splitting under different conditions with lower onset potential and overpotential compared than those of RuCu NPs/C and commercial Ir/C||Pt/C. The RuCu NSs/C also exhibits excellent stability with small potential change during chronoamperometry measurement in both 1 M KOH and 0.5 M H_2SO_4. DFT calculations reveal that the channel-rich RuCu NSs possesses not only the highly active electron transfer between key intermediates but also optimize the electronic structures of both oxidation ability of Ru and reduction ability of Cu for the universal water-splitting. These promising results highlight that 2D Ru-based electrocatalysts are promising functional electrocatalysts for overall water splitting.

Acknowledgements

This work was financially supported by the Ministry of Science and Technology (2016YFA0204100, 2017YFA0208200), the National Natural Science Foundation of China (21571135), Young Thousand Talented Program, Jiangsu Province Natural Science Fund for Distinguished Young Scholars (BK20170003), the Priority Academic Program Development of Jiangsu Higher Education Institutions (PAPD), and the start-up funding from Soochow University.

Keywords: Channel • Ru • Nanosheet • pH-Universal • Overall water splitting

[1] Z. W. Seh, J. Kibsgaard, C. F. Dickens, I. Chorkendorff, J. K. Norskov, T. F. Jaramillo, *Science* **2017**, *355*. 146.

[2] B. Rausch, M. D. Symes, G. Chisholm, L. Cronin, *Science* **2014**, *345*, 1326.

[3] J. Wang, W. Cui, Q. Liu, Z. Xing, A. M. Asiri, X. Sun, *Adv. Mater*. **2016**, *28*, 215-230.

[4] Y. H. Li, P. F. Liu, L. F. Pan, H. F. Wang, Z. Z. Yang, L. R. Zheng, P. Hu, H. J. Zhao, L. Gu, H. G. Yang, *Nat. Commun.* **2015**, *6*, 8064.

[5] W. Zhou, X.-J. Wu, X. Cao, X. Huang, C. Tan, J. Tian, H. Liu, J. Wang, H. Zhang, *Energy Environ. Sci*. **2013**, *6*, 2921-2924.

[6] X. Gao, H. Zhang, Q. Li, X. Yu, Z. Hong, X. Zhang, C. Liang, Z. Lin, *Angew. Chem. Int. Ed.* **2016**, *55*, 6290-6294.
[7] J. Hou, B. Zhang, Z. Li, S. Cao, Y. Sun, Y. Wu, Z. Gao, L. Sun, *ACS Catal*. **2018**, *8*, 4612-4621.
[8] M. Gong, W. Zhou, M. C. Tsai, J. Zhou, M. Guan, M. C. Lin, B. Zhang, Y. Hu, D. Y. Wang, J. Yang, S. J. Pennycook, B. J. Hwang, H. Dai, *Nat. Commun.* **2014**, *5*, 4695.
[9] Y. Yan, B. Xia, Z. Xu, X. Wang, *ACS Catal.* **2014**, *4*, 1693-1705.
[10] T. Wang, C. Wang, Y. Jin, A. Sviripa, J. Liang, J. Han, Y. Huang, Q. Li, G. Wu, *J. Mater. Chem. A* **2017**, *5*, 25378-25384.
[11] Y. Jiao, Y. Zheng, M. Jaroniec, S. Z. Qiao, *Chem. Soc. Rev*. **2015**, *44*, 2060-2086.
[12] E. Antolini, *ACS Catal.* **2014**, *4*, 1426-1440.
[13] J. Zhang, T. Wang, D. Pohl, B. Rellinghaus, R. Dong, S. Liu, X. Zhuang, X. Feng, *Angew. Chem. Int. Ed.* **2016**, *55*, 6702-6707.
[14] L. Fan, P. F. Liu, X. Yan, L. Gu, Z. Z. Yang, H. G. Yang, S. Qiu, X. Yao, *Nat Commun.* **2016**, *7*, 10667.
[15] Z. Geng, Y. Liu, X. Kong, P. Li, K. Li, Z. Liu, J. Du, M. Shu, R. Si, J. Zeng, *Adv. Mater.* **2018**, *30*, 1803498
[16] X. Cui, A. E. Surkus, K. Junge, C. Topf, J. Radnik, C. Kreyenschulte, M. Beller, *Nat. Commun.* **2016**, *7*, 11326.
[17] Y. Liu, S. Liu, Y. Wang, Q. Zhang, L. Gu, S. Zhao, D. Xu, Y. Li, J. Bao, Z. Dai, *J. Am. Chem. Soc.* **2018**, *140*, 2731-2734.
[18] L. Gloag, T. M. Benedetti, S. Cheong, Y. Li, X. H. Chan, L. M. Lacroix, S. L. Y. Chang, R. Arenal, I. Florea, H. Barron, A. S. Barnard, A. M. Henning, C. Zhao, W. Schuhmann, J. J. Gooding, R. D. Tilley, *Angew. Chem. Int. Ed.* **2018**, *57*, 10241-10245.
[19] J. Su, Y. Yang, G. Xia, J. Chen, P. Jiang, Q. Chen, *Nat. Commun.* **2017**, *8*, 14969.
[20] J. Liu, Y. Zheng, Y. Jiao, Z. Wang, Z. Lu, A. Vasileff, S. Z. Qiao, *Small* **2018**, *14*, e1704073.
[21] J. Su, R. Ge, K. Jiang, Y. Dong, F. Hao, Z. Tian, G. Chen, L. Chen, *Adv. Mater.* **2018**, 30, 1801351.
[22] L. Wang, Y. Zhang, L. Chen, H. Xu, Y. Xiong, *Adv. Mater.* **2018**, e1801955.
[23] S. W. Liu, Hk. P. Wang, Q. Xu, T. B. Ma, G. Yu, C. Zhang, D. Geng, Z. Yu, S. Zhang, W. Wang, Y. Z. Hu, H. Wang, J. Luo, *Nat. Commun.* **2017**, *8*, 14029.
[24] X. Hong, C. Tan, J. Chen, Z. Xu, H. Zhang, *Nano Research* **2014**, *8*, 40-55.
[25] S. Sun, H. Li, Z. J. Xu, *Joule* **2018**, *2*, 1024-1027.

[26] C. Zhu, Q. Shi, S. Fu, J. Song, H. Xia, D. Du, Y. Lin, *Adv. Mater.* **2016**, *28*, 8779-8783.
[27] J. Yu, Y. Zhong, X. Wu, J. Sunarso, M. Ni, W. Zhou, Z. Shao, *Adv. Sci.* **2018**, *5*, 1800514.
[28] R. Ma, Y. Zhou, Y. Chen, P. Li, Q. Liu, J. Wang, *Angew. Chem. Int. Ed.* **2015**, *54*, 14723-14727.
[29] P. Xiao, M. A. Sk, L. Thia, X. Ge, R. J. Lim, J.-Y. Wang, K. H. Lim, X. Wang, *Energy Environ. Sci.* **2014**, *7*, 2624-2629.
[30] Y. Jin, H. Wang, J. Li, X. Yue, Y. Han, P. K. Shen, Y. Cui, *Adv. Mater.* **2016**, *28*, 3785-3790.
[31] Z. Zhang, Y. Liu, B. Chen, Y. Gong, L. Gu, Z. Fan, N. Yang, Z. Lai, Y. Chen, J. Wang, Y. Huang, M. Sindoro, W. Niu, B. Li, Y. Zong, Y. Yang, X. Huang, F. Huo, W. Huang, H. Zhang, *Adv. Mater.* **2016**, *28*, 10282-10286.
[32] K. Sardar, E. Petrucco, C. I. Hiley, J. D. Sharman, P. P. Wells, A. E. Russell, R. J. Kashtiban, J. Sloan, R. I. Walton, *Angew. Chem. Int. Ed*. **2014**, *53*, 10960-10964.
[33] L. Shi, T. Zhao, A. Xu, Z. Wei, *ACS Catal.* **2016**, *6*, 6285-6293.
[34] E. Yilmaz, C. Yogi, K. Yamanaka, T. Ohta, H. R. Byon, *Nano Lett.* **2013***, 13,* 4679-4684*.*
[35] B. Lu, L. Guo, F. Wu, Y. Peng, J. E. Lu, T. J. Smart, N. Wang, Y. Z. Finfrock, D. Morris, P. Zhang, N. Li, P. Gao, Y. Ping, S. Chen, *Nat. Commun.* **2019**, *10*, 63

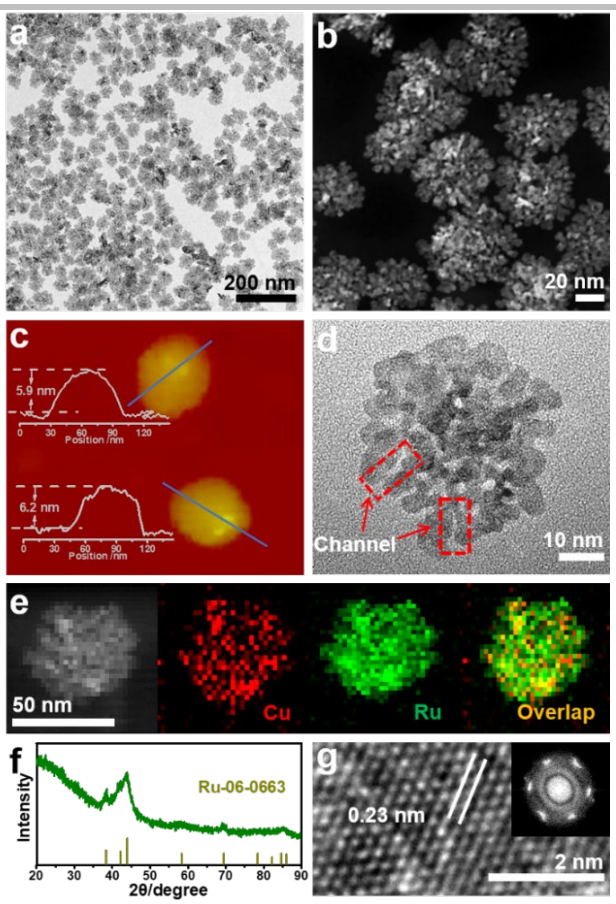

Figure 1. (a) TEM image, (b) HAADF-STEM image, (c) AFM images and corresponding thickness, (d) High-magnification TEM image, (e) HAADF-STEM-EDS elemental mappings, (f) XRD pattern and (g) HRTEM image and associated FFT of RuCu NSs.

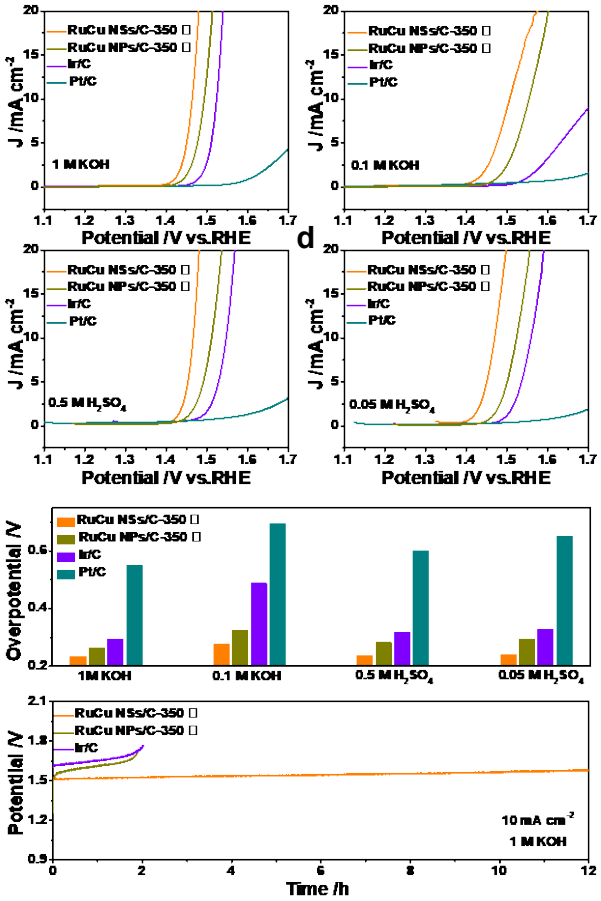

Figure 2. OER activities of RuCu NSs/C-350 °C, RuCu NPs/C-350 °C, Ir/C and Pt/C in (a) 1 M KOH, (b) 0.1 M KOH, (c) 0.5 M H_2SO_4 and (d) 0.05 M H_2SO_4. (e) Overpotentials of different electrocatalysts in different electrolytes at 10 mA cm^{-2}. (f) Chronopotentiometry tests of RuCu NSs/C-350 °C, RuCu NPs/C-350 °C and Ir/C in 1 M KOH at 10 mA cm^{-2}.

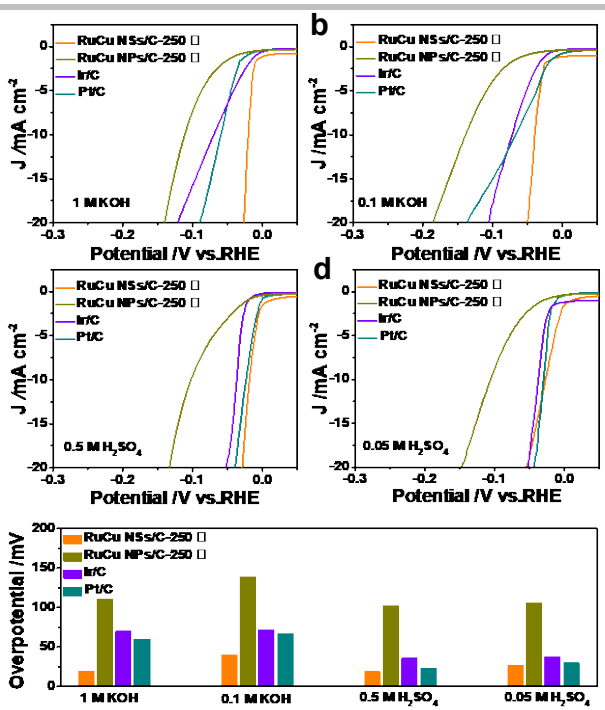

Figure 3. HER activity of RuCu NSs/C-250 °C, RuCu NPs/C-250 °C, Ir/C and Pt/C in (a) 1 M KOH, (b) 0.1 M KOH, (c) 0.5 M H_2SO_4 and (d) 0.05 M H_2SO_4. (e) Overpotentials of RuCu NSs/C-250 °C, RuCu NPs/C-250 °C, Ir/C and Pt/C in different electrolytes at 10 mA cm^{-2}.

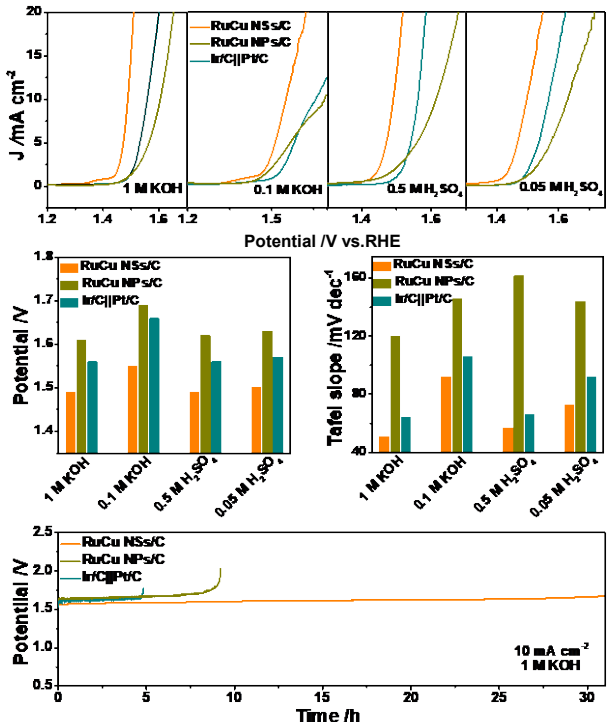

Figure 4. Polarization curves of RuCu NSs/C, RuCu NPs/C and Ir/C||Pt/C for overall water splitting in (a) 1 M KOH, 0.1 M KOH, 0.5 M H_2SO_4 and 0.05 M H_2SO_4, respectively. (b) Potentials and (c) Tafel slopes of RuCu NSs/C, RuCu NPs/C and Ir/C||Pt/C in different electrolytes calculated from corresponding polarization curves**.** (d) Chronopotentiometry tests of RuCu NSs/C, RuCu NPs/C and Ir/C||Pt/C in 1 M KOH at 10 mA cm^{-2}.

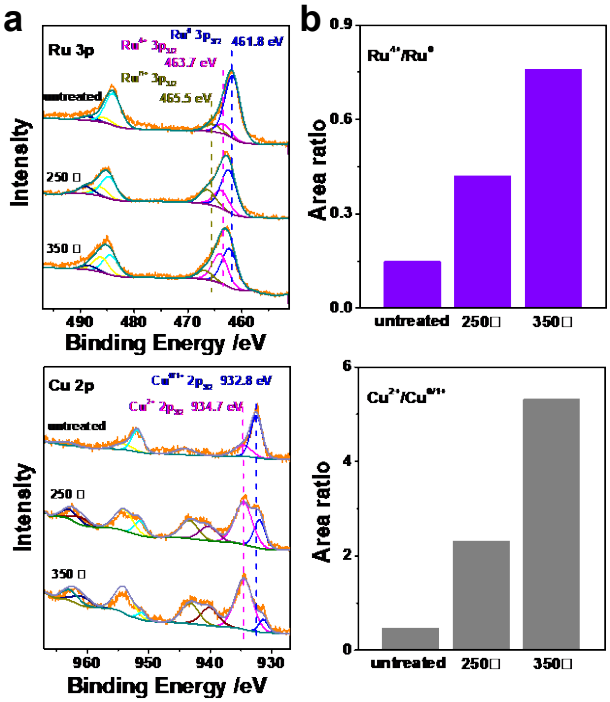

Figure 5. (a) Ru 3p XPS spectra. (b) corresponding area ratios of Ru^{4+}/Ru^{0}.(c) Cu 2p XPS spectra and (d) corresponding area ratios of $Cu^{2+}/Cu^{0/1+}$.